Hindawi Publishing Corporation
Advances in Materials Science and Engineering
Volume 2015, Article ID 163205, 17 pages
http://dx.doi.org/10.1155/2015/163205

Research Article

Atmospheric Corrosion Behavior of 2A12 Aluminum Alloy in a Tropical Marine Environment

Zhongyu Cui,[1,2] Xiaogang Li,[1] Huan Zhang,[1] Kui Xiao,[1] Chaofang Dong,[1] Zhiyong Liu,[1] and Liwei Wang[3]

[1]*Corrosion and Protection Center, University of Science and Technology Beijing, Beijing 100083, China*
[2]*Institute of Materials Science and Engineering, Ocean University of China, Qingdao 266100, China*
[3]*Pipeline Research Institute of China National Petroleum Corporation, Langfang 065000, China*

Correspondence should be addressed to Xiaogang Li; lixiaogang@ustb.edu.cn

Received 2 March 2015; Accepted 31 May 2015

Academic Editor: Somchai Thongtem

Atmospheric corrosion behavior of 2A12 aluminum alloy exposed to a tropical marine environment for 4 years was investigated. Weight loss of 2A12 alloy in the log-log coordinates can be well fitted with two linear segments, attributing to the evolution of the corrosion products. EIS results indicate that the corrosion product layer formed on the specimens exposed for 12 months or longer presents a good barrier effect. Corrosion morphology changes from pitting corrosion to severe intergranular corrosion with the extension of exposure time, resulting in the reduction of the mechanical properties.

1. Introduction

Due to their high strength and low density, 2xxx series aluminum alloys have been extensively used as structural materials in the aircraft and aerospace industries [1, 2]. However, they are prone to different forms of corrosion, such as pitting corrosion, intergranular corrosion, exfoliation corrosion, and even stress corrosion cracking when exposed in outdoor atmosphere especially in marine atmosphere.

Atmospheric corrosion studies have been conducted on aluminum alloys in laboratory controlled environments [3–5]. The main focus was on the effects of environmental factors, such as relative humidity (RH), chloride contents, CO_2, and SO_2. Sun et al. [4] investigated the exfoliation corrosion of extruded 2024-T4 by laboratory-accelerated test and found that exfoliation could occur when the RH was higher than 75%, and the higher the temperature or the Cl^- amount was, the more serious exfoliation the specimen suffered. Blücher et al. [5] investigated the effect of CO_2 on the NaCl-induced atmospheric corrosion of AA 1070 aluminum and demonstrated that corrosion is about 10–20 times faster in CO_2-free humid air compared with air containing ambient levels of CO_2. However, the laboratory simulation tests are not sufficient for predicting actual service performance of aluminum alloys because of the differences in environment, and field exposure tests are needed.

Some field exposure tests have been conducted on aluminum alloys in various atmospheric environments and pitting corrosion [6–9], intergranular corrosion [7], exfoliation corrosion [4, 9], and stress corrosion cracking [7] have been detected. It has been illustrated that atmospheric corrosion is more serious for high strength aluminum alloys because of the addition of some alloy elements which can form second phases and accelerate the localized corrosion. For instance, Sun et al. [9] investigated atmospheric corrosion behavior of 2024 and 7075 aluminum alloys in urban, coastal, and industrial environments for 20 years. The results showed that exfoliation corrosion occurred on extruded 2024 and 7075 aluminum alloys in coastal and industrial atmospheres, and mechanical properties decreased greatly with the occurrence of exfoliation. Wang et al. [7] investigated the atmospheric corrosion of 2024-T3 alloy exposed to salt lake environment and found that weight loss of the alloy monotonically increased as exposure time prolonged in the first 2 years and then tended to be stable over time. Generally, the stabilization of weight loss during long-term exposure was attributed

Table 1: Chemical composition of 2A12 aluminum alloy used in this work.

Alloy	Chemical composition (wt.%)							
	Si	Fe	Cu	Mn	Mg	Zn	Ti	Al
2A12	0.13	0.35	4.68	0.53	1.58	0.10	0.023	Bal.

to the formation of a layer of oxide film on the surface which could control the diffusion of the reaction species and inhibit the corrosion process [10]. The relationship between the protectiveness of corrosion products and the weight loss has been investigated by using electrochemical techniques [8, 11]. Liu et al. [8] investigated the influence of native oxide and corrosion products on atmospheric corrosion of pure Al through electrochemical impedance spectroscopy (EIS). They revealed that the structure and thickness of the native oxide and corrosion products were the main factors that influenced the atmospheric corrosion of pure Al. Vilche et al. [11] indicated that a bilayer structure formed on the surface of pure Al exposed to aggressive sites for 2 years by using EIS.

In this work, corrosion behavior of 2A12 aluminum alloy exposed in a tropical marine atmosphere for 4 years was investigated. The corrosion rate was determined by the weight loss method. The composition, structure, and protectiveness of the corrosion products were characterized with morphology analysis and EIS. The corrosion kinetics, the protectiveness of the corrosion products, and the corrosion mechanisms of this alloy in tropical marine atmosphere were discussed.

2. Experimental Details

2.1. Materials Preparation. A sheet of 2A12 aluminum alloy was used in this work. Chemical composition of the 2A12 alloy was listed in Table 1. Samples were wet-ground through successive grades of silicon carbide abrasive papers from P120 to P2000 followed by diamond finishing to 0.1 mm. Then the specimen was subjected to a scanning electron microscope (SEM, Quanta 250) to observe the distribution and compositions of the second phases. For the metallographic characterization, the polished surface was further etched using Keller's reagent with the following composition: 1 mL hydrofluoric acid (HF), 1.5 mL hydrochloric acid (HCl), 2.5 mL nitric acid (HNO_3), and 95 mL water (H_2O). After ultrasonic cleaning in ethanol for 1 min and drying in air, the samples were taken immediately to a KEYENCE VHX2000 stereology microscope for microstructure observation. The microstructure of the 2A12 alloy was further investigated by transmission electron microscopy (TEM; Tecnai G^2 F20), with the work function of 300 kV. Thin foils for TEM were cut to about 500 μm by an electron discharge cutter and later ground and polished on both sides to a thickness of about 70 μm. Then the thin foils were ion-milled at room temperature in a Gatan PIPS with a small incident angle until perforation.

Figure 1 showed the optical micrograph (a) of the 2A12 aluminum alloy and the distribution (b) and composition ((c) and (d)) of the second phases. The grain size of this alloy varied between 20 and 200 μm (Figure 1(a)) with many intermetallic (IM) particles locating in the substrate (white particles in Figure 1(b)). EDS results indicated that these particles were mainly composed of Al_2CuMg (Figure 1(c)) and AlCuFeMn(Si) (Figure 1(d)) which was consistent with the results of Chen et al. [12].

Figure 2 showed the TEM images of the IM particles and the grain boundary zones. Figure 2(a) was a typical rod-like particle which distributed in the grain. According to the selected area electron diffraction result and the previous studies [13, 14], this phase was the Mn-rich T ($Al_{20}Cu_2Mn_3$) dispersoid which usually formed in the ingot homogenization process and could refine the grain through the way of pinning grain boundary migration during recrystallization annealing process [14]. As shown in Figure 2(b), this phase was also found along the grain boundaries. Figure 2(c) showed an IM particle at the grain boundary, which was identified as *S* phase (Al_2CuMg) based on the selected area diffraction pattern. This kind of phase played an important role in the pitting corrosion and intergranular corrosion of aluminum alloys [15]. In addition, it is worthwhile to note that precipitate-free zone (PFZ) was not found in this alloy. Instead, there are some clean grain boundaries without precipitation particles as shown in Figure 2(d).

2.2. Field Exposure Test. Samples with the dimension of 100 mm × 50 mm × 2.5 mm were used for field exposure test. Prior to the test, all the specimens were ground down to 800 grit paper and then degreased by acetone followed by cleaning in ethanol. All the specimens were weighed (original weight) and the surface area (*S*) was measured before test. Then all the specimens were installed on a test rack with an inclination angle of 45° horizontal to the sky and facing south in Xisha islands (112°20′E, 16°50′N), 100 meters from the coastline. The test duration was 4 years. Four replicate metal samples were retrieved from the exposure site after 1, 3, 6, 9, 12, 24, and 48 months. Three replicas were employed to determine the weight loss, and the remaining one was used to analyze the corrosion morphology and the corrosion products.

Table 2 lists the annual average environmental parameters and atmospheric pollutants measured at Xisha islands during the exposure, which is consistent with the description in our previous work [16]. The annual average temperature in Xisha marine atmosphere was 27°C with the maximum temperature increasing up to 33.3°C and the minimum temperature reducing to 20.1°C which was also a relatively high temperature. The extreme relative humidity (RH) values oscillated between 61% and 94% with a mean value of 77%. Time of wetness, which was defined as the period during which a metallic surface was covered by adsorptive and/or liquid film of electrolyte, was another important factor that affects the corrosion behavior of metals in atmosphere. Schindelholz et al. [17] summarized that the TOW determination methods represented in the literature and practice could be categorized by the way in which TOW was treated either as an environmental parameter or as a surface parameter. However, both of the two methods including ISO 9223 and other indirect electrode sensors had their limitations [18, 19]. In this work, the TOW was treated as an environmental parameter

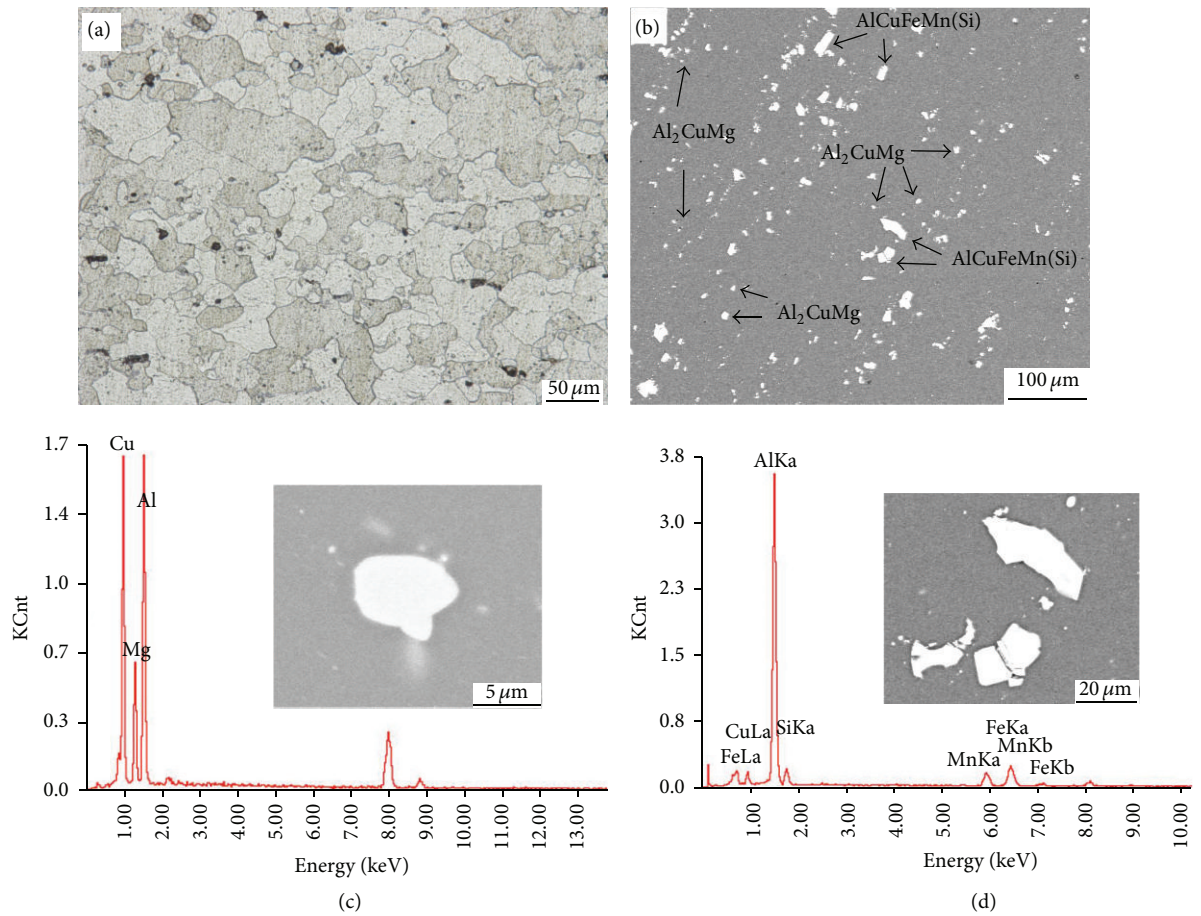

Figure 1: Microstructure of 2A12 aluminum alloy used in this work: (a) optical micrograph, (b) SEM images of the distribution of second phases, (c) EDS of AlCuMg particles, and (d) EDS of AlCuFeMnSi particles.

Table 2: Climatic parameters and atmospheric pollutants of Xisha islands during 4 years of exposure.

Exposure site	Xisha	TOW	2562 h/year (τ_4)
Location	112°20′E, 16°50′N	Rainfall	1526 mm/year
Max. temperature	33.3°C	Cl^- deposition rate	112.68 mg/m^2 d (S_2)
Min. temperature	20.1°C	SO_2 deposition rate	<0.1 mg/m^2 d (P_0)
Average temperature	27°C	Sunshine	2675 h/year
Max. RH	94%	pH of rain	6.5
Min. RH	61%	Distance to sea	100 m
Average RH	77%		

and was calculated according to ISO 9223, which defines TOW as the length of time when the RH is greater than 80% at a temperature above 0°C. With this method, the approximate TOW in Xisha islands was 2562 h/year which belonged to the classification of τ_4 [20]. As for the corrosive species precipitated on the samples, the Cl^- and SO_2 deposition rates were considered and measured using the method given by ISO 9225 [21]. The Cl^- deposition rate was determined by the wet candle method and the SO_2 deposition rate was determined using alkaline surfaces of porous filter plates saturated by a solution of sodium carbonate. According to the results, the annual average deposition rate of chloride was 112.68 mg/m^2 d, which was classified under S_2 [20]. Meanwhile, the precipitation of SO_2 was less than 0.1 mg/m^2·d and the rain had a near-neutral pH of 6.5 because of the absence of heavy industry at the exposure site.

Figure 3 showed the monthly average temperature, RH, TOW, and Cl^- deposition rate during the exposure test. The temperature presented a seasonal characteristic with a higher value in summer and lower value in winter (Figure 3(a)). As for the RH and TOW, the highest value all appeared at October, while the gap between other months was not so great (Figures 3(b) and 3(c)). In addition, variation of the Cl^- deposition rate exhibited no trend here. It fluctuated with

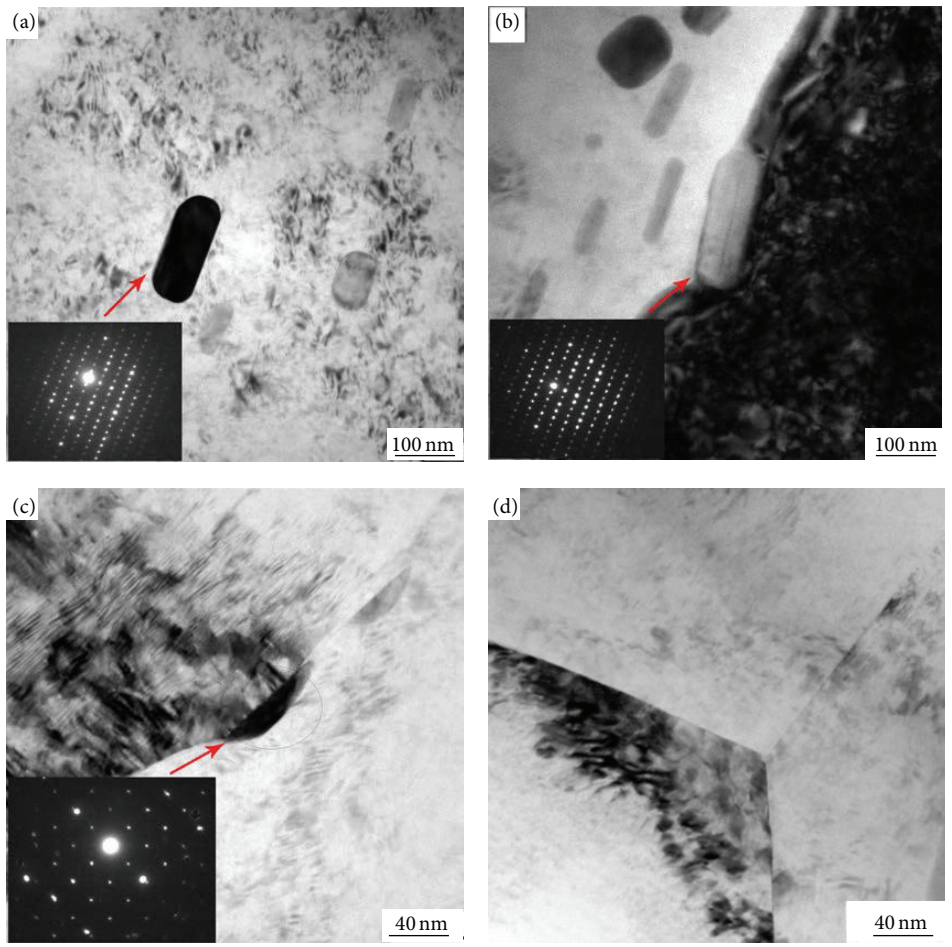

Figure 2: TEM images of the intermetallic precipitates in the matrix (a), along the grain boundaries (b, c) and the clean grain boundaries (d).

the exposure time with a higher value in the second half of one year (Figure 3(d)).

2.3. Weight Loss Measurement. Corrosion products of the withdrawn triplicate specimens were chemically removed by pickling in the solution (50 mL H_3PO_4 + 20 g CrO_3 + 1 L H_2O) for 10 min at 80–100°C. After that, the specimens were rinsed with distilled water, dried in warm air, and then weighed to obtain their final weights (w_1). Meanwhile, the metal loss caused by picking was determined by using uncorroded sample. Then, the weight loss was calculated as follows:

$$W = \frac{w_0 - w_1}{S} - W_{un}, \quad (1)$$

where W was the weight loss of the metal due to corrosion (g/m^2), w_0 was the original weight (g), w_1 was the final weight (g), W_{un} was the weight loss of a fresh specimen due to the picking, and S was the surface area (m^2). The average corrosion rate of aluminum after exposure for different periods was calculated by using the equation in [22]:

$$V_n = \frac{12\,(w_n - w_{n-1})}{t_n - t_{n-1}}, \quad (2)$$

where V_n was the corrosion rate (g/m^2·year), w_n was the weight loss (g/m^2), t was the exposure time (month), and n was the period of exposure (n = 1, 2, 3, 4, 5, 6, and 7 referred to the sample exposed for 1, 3, 6, 9, 12, 24, and 48 months, resp.).

2.4. Mechanical Properties Measurement. After removing the corrosion products, the corroded tensile specimens were machined according to the ASTM E8M specification with 25 mm gauge length and 6 mm gauge width, and the thickness remained unchanged. Then, the tensile tests were carried out according to ASTM E8M with a constant deformation rate of 1 mm/min. A data logger was used to store the data in a digital file. To get representative average values of the tensile properties, three tensile tests have been carried out per each test series.

2.5. Characterization of Corrosion Morphology and Corrosion Products. After the exposure test, the macroscopic appearances of the specimens with corrosion products were taken by a D200 digital camera. Then, the microscopic corrosion morphologies with and without corrosion products were observed by scanning electron microscope (SEM,

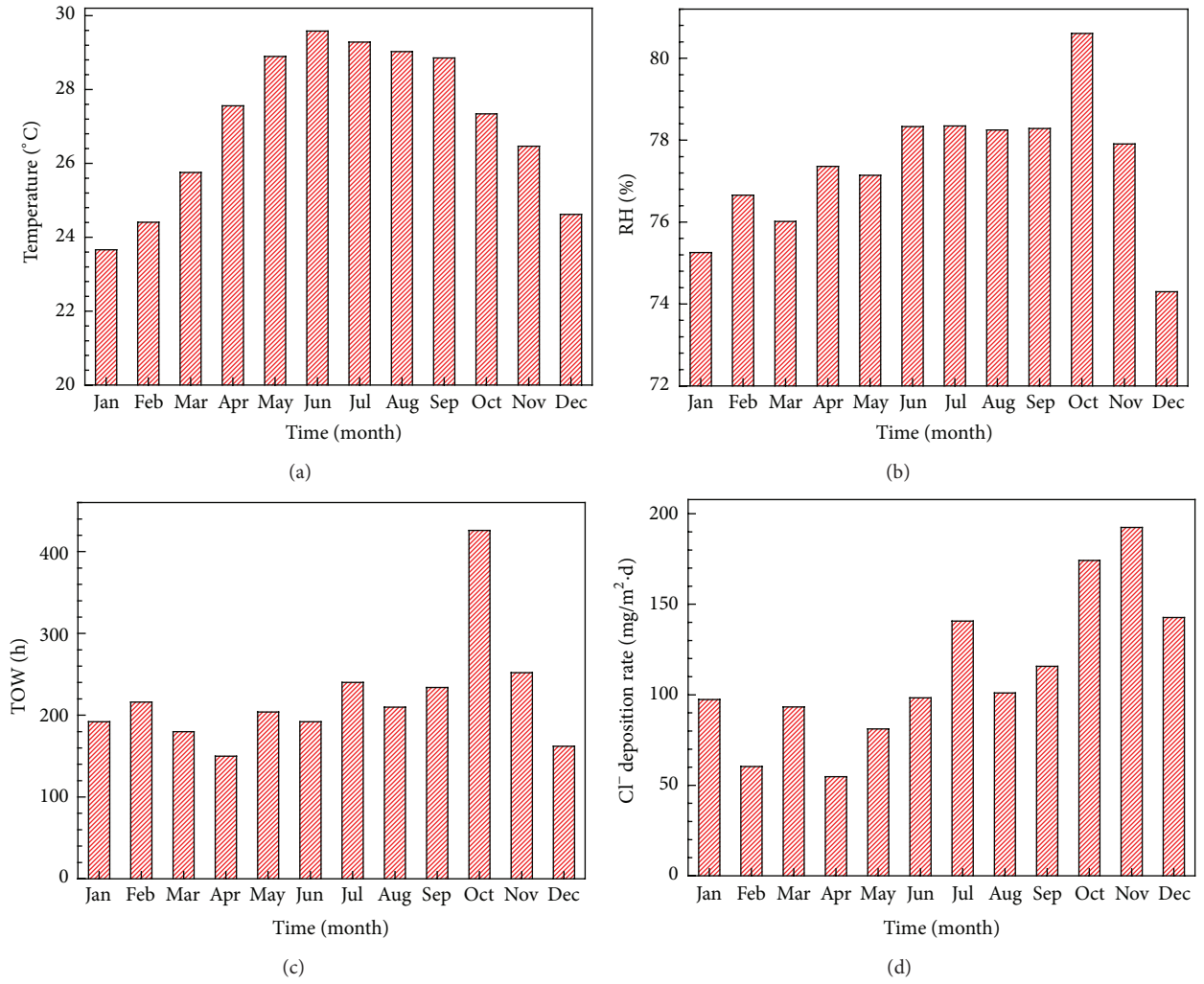

Figure 3: Monthly average temperature (a), RH (b), TOW (c), and Cl^- deposition rate (d) during the exposure test.

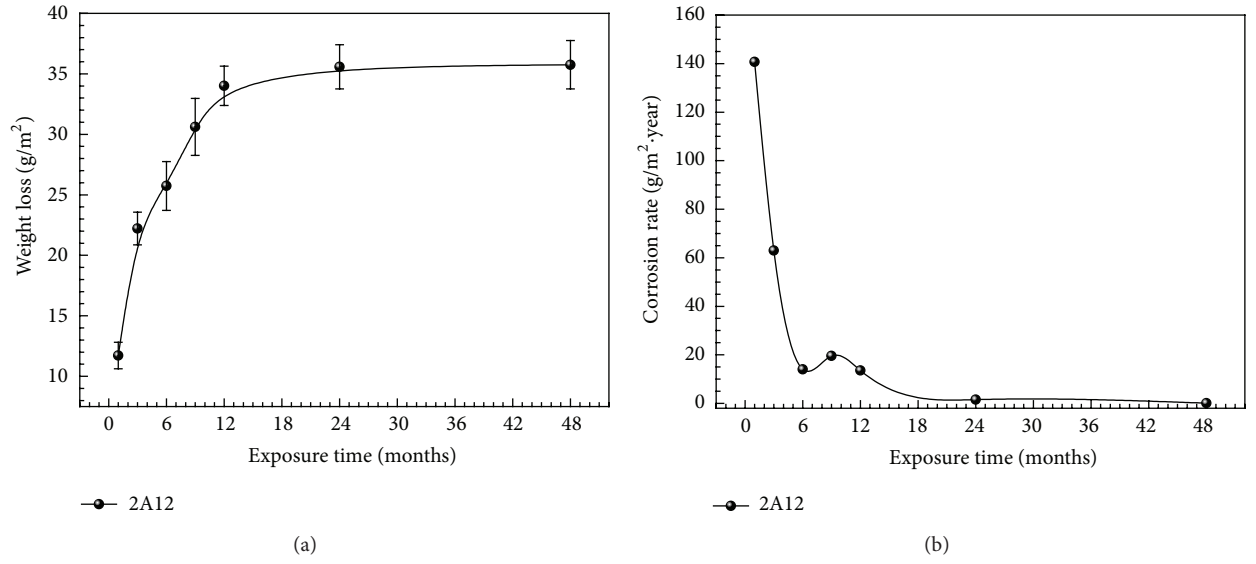

Figure 4: Weight loss (a) and corrosion rate (b) of 2A12 aluminum alloy during exposure in Xisha marine atmosphere for 4 years.

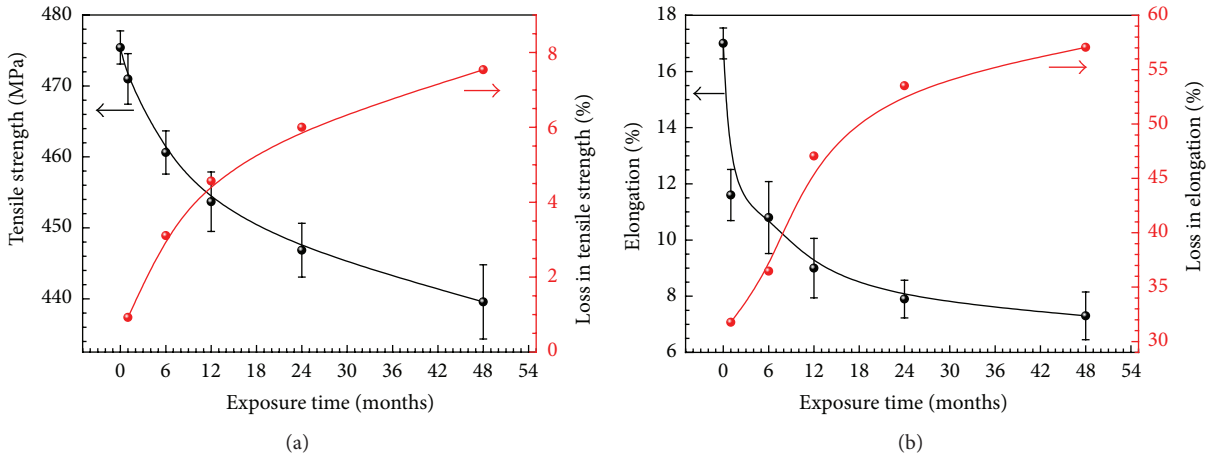

FIGURE 5: Changes of the tensile strength (a) and elongation (b) of 2A12 alloy exposed for different time.

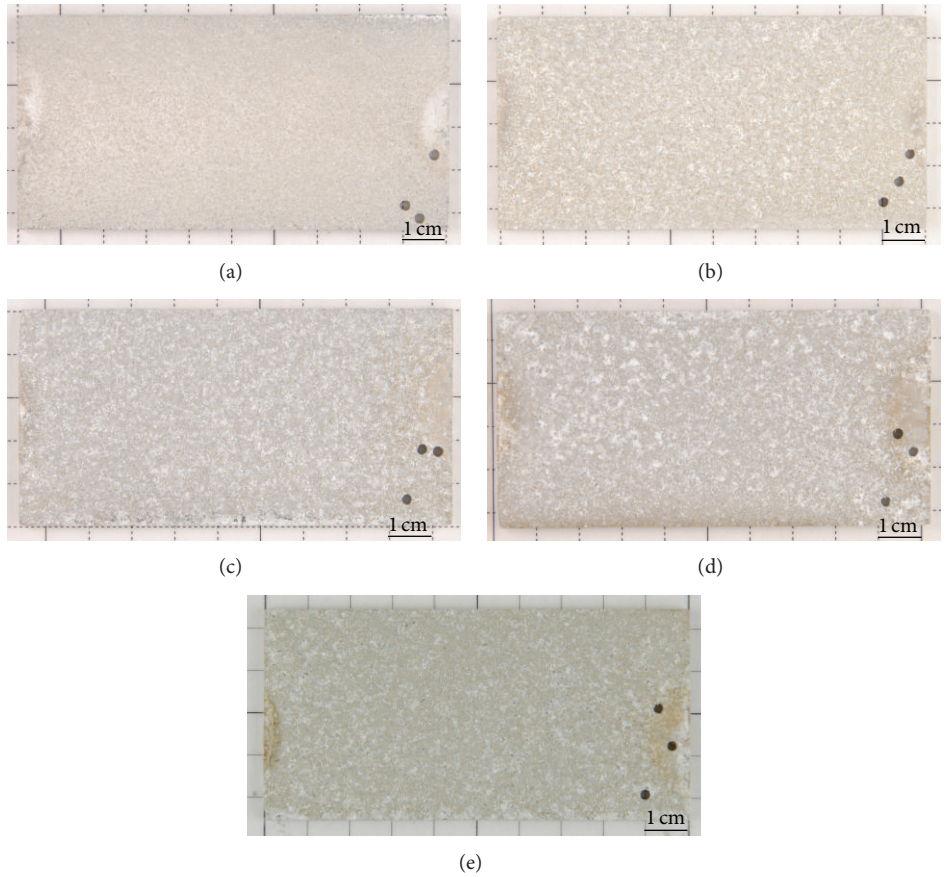

FIGURE 6: Surface appearances of the 2A12 aluminum alloy exposed for 1 month (a), 6 months (b), 12 months (c), 24 months (d), and 48 months (e).

Quanta 250). Element compositions of the corrosion products were analyzed by energy dispersive X-ray spectroscopy (EDS). Elemental distributions in the corrosion product layer were examined by electron probe microanalyzer (EPMA, JXA8230) with accelerating voltage of 15 kV and sample current of 0.02 μA. Before the EPMA experiment, the specimen with corrosion products was embedded in the epoxy resin. Then the specimen was mechanically ground down to 2000 grit SiC paper and polished with 1.5 μm diamond paste. The X-ray diffraction (XRD, Rigaku Dmax-rc) investigation was carried out in situ on the exposed specimens and conducted in a step scanning mode from 10° to 90° with Cu Kα radiation. After that, the data was analyzed with Jade 5.0 software.

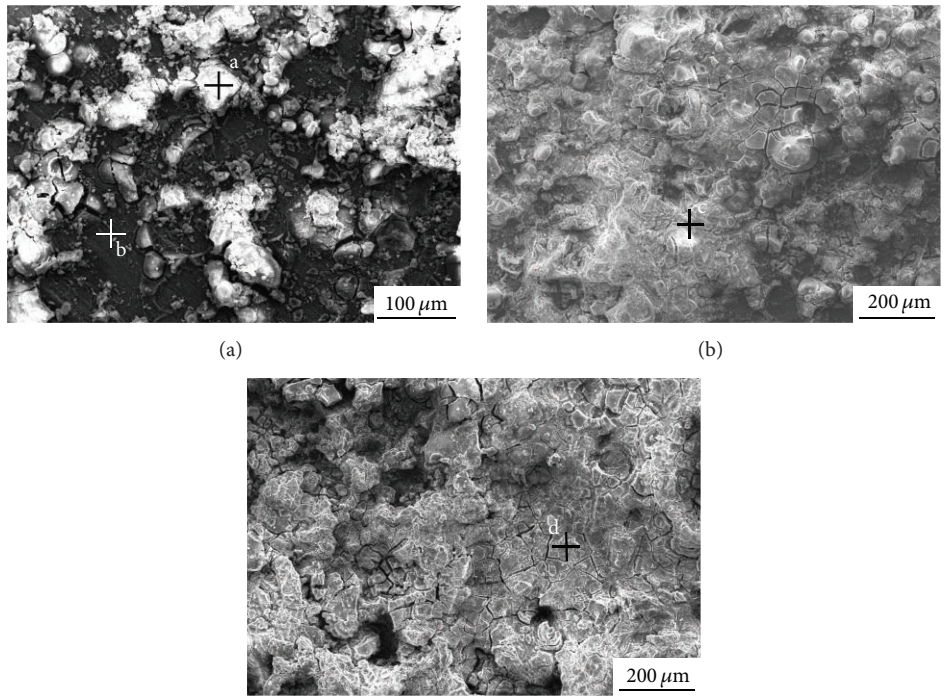

Figure 7: Surface morphology of the corrosion products formed on 2A12 aluminum alloy after exposure for 1 month (a), 12 months (b), and 48 months (c).

2.6. Electrochemical Impedance Spectroscopy (EIS) Measurement. EIS measurements were performed with VMP3 electrochemical workstation in 0.1 M NaCl solution in a conventional three-electrode cell, using a platinum sheet as counter electrode and a saturated calomel electrode (SCE) as reference electrode. The test system was always in a steady state with no stirring. The whole metal sample was manually sectioned into coupons of dimensions 15 mm × 15 mm × 2.5 mm which served as working electrode. The working electrode surface was covered with silicone rubber leaving an exposed area of 1.0 cm^2. The impedance spectra were recorded in the frequency range between 100 kHz and 10 mHz with 10 mV amplitude peak to peak perturbing signal. The experimental data were analyzed by the commercial software ZSimpWin. All the measurements were performed at ambient temperature (25 ± 2°C) and repeated at least three times to maintain the reproducibility.

3. Results

3.1. Weight Loss and Corrosion Rate. Figure 4 shows the weight loss (a) and the corrosion rate (b) of 2A12 aluminum alloy during the 4-year exposure in Xisha marine atmosphere. An increasing trend in weight loss consisting of two different segments is observed in Figure 4(a). The weight loss increases rapidly during the initial 12 months of exposure and then the increasing rate decreases to a much lower value as the exposure time prolonged. Corrosion rate of the alloy decreases remarkably at the initial six months of exposure and then presents a slight augment from 6 months to 9 months. With further increasing of the weathering test, corrosion rate decreases gradually and stabilizes to a certain value. Corrosivity of aluminum alloys in atmospheric environment has been classified into five grades in some literatures [3, 9, 23] according to ISO 9223. The corrosion rate of 2A12 alloy after exposure in Xisha islands for 1 year is 34.49 g/m^2·year, so it belongs to the classification of C_5 (very high) based on ISO 9223 [20].

3.2. Loss in Mechanical Properties. Changes of the tensile strength and elongation for 2A12 alloy versus exposure time in Xisha marine atmosphere are shown in Figure 5. The tensile strength decreases gradually as the exposure test extends (Figure 5(a)). The biggest loss is about 40 MPa and 7.6% in percentage. As for the elongation, it reduces from 17% for the uncorroded specimen to 7.3% for the specimen exposed for 48 months. That is, the toughness loss reaches 57% in the end of the exposure test. The reduction in mechanical properties has been reported by many literatures [24, 25]. This reduction can be attributed either to hydrogen embrittlement or to the stress concentration of the corrosion-induced intergranular cracks [24].

3.3. Macroscopic Appearances. Figure 6 shows the macroscopic appearances of the 2A12 specimens exposed for different time. The surfaces are covered with corrosion products so that the original appearances of the samples cannot be seen. It is seen that the specimens become grey with increasing of the exposure time and the corrosion product layers are relatively uniform.

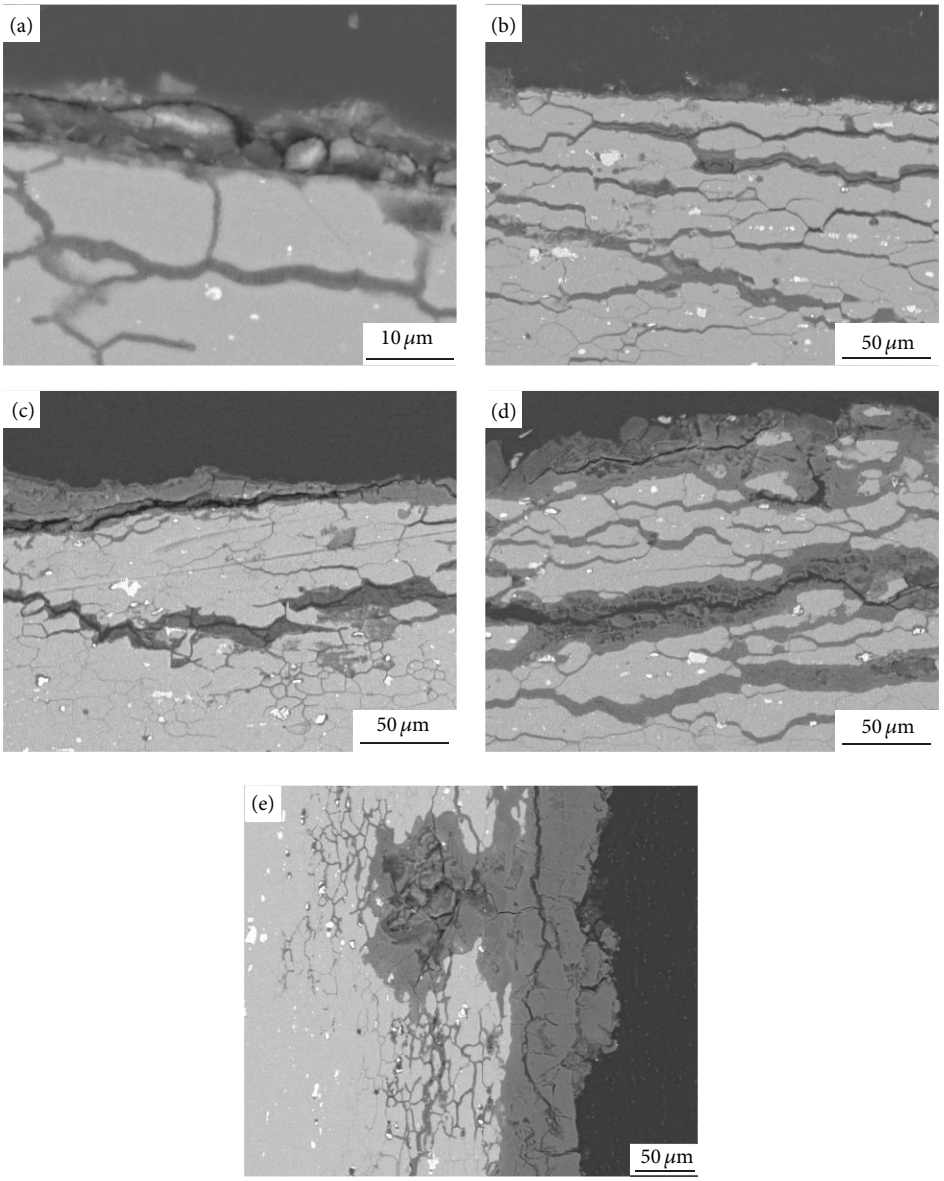

Figure 8: Cross-sectional morphology of 2A12 aluminum alloy after exposure for 1 month (a), 6 months (b), 12 months (c), 24 months (d), and 48 months (e).

3.4. Corrosion Product Analysis

3.4.1. Surface Morphology. Figure 7 shows the surface morphologies of the corrosion products formed on 2A12 aluminum alloy after exposure for different time. The images demonstrate that many microcracks exist in the corrosion products which are mainly attributed to the dehydration process during the wet-dry cycles [22]. The chemical compositions of the points a, b, c, and d marked in Figure 7 are listed in Table 3. The primary elements included in the corrosion products are Al and O, with a trace amount of Mg, Na, Cl, and Ca, which mainly come from the salt particles that deposited on the surface of the metal.

3.4.2. Cross-Sectional Morphology. Cross-sectional morphologies of the corrosion product layer on 2A12 aluminum alloy after exposure for different time are shown in Figure 8. It can be seen that intergranular corrosion occurs on the specimen after only 1 month of exposure (Figure 8(a)). As the weathering time prolonged, the intergranular corrosion

Table 3: Element contents of corrosion products marked in Figure 4 determined by EDS.

Point	Chemical composition (wt.%)					
	O	Al	Mg	Na	Cl	Ca
a	67.21	27.84	1.21	0.98	1.16	1.60
b	22.73	75.35	1.92	—	—	—
c	65.49	34.51	—	—	—	—
d	64.23	34.71	1.07	—	—	—

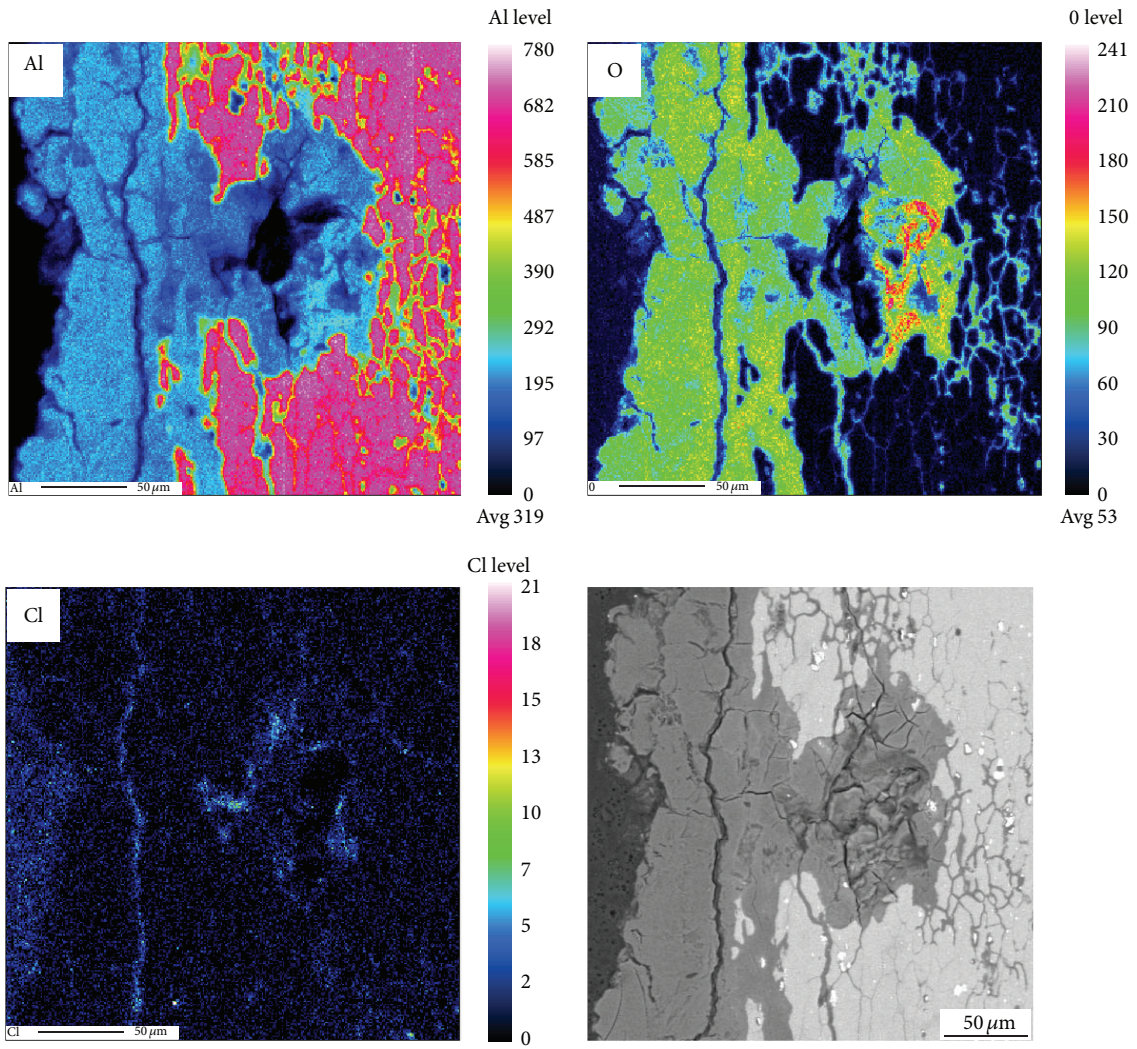

Figure 9: EPMA mapping of the main elements distributing on the cross section of the specimen after exposure for 48 months.

crack width increases. After exposure for 48 months, the specimen surface is covered by a compact and thick corrosion product layer under which there exist some isolated pits. To determine the distribution of the elements on the corrosion products of 2A12 aluminum alloy, the EPMA map scanning analysis is performed and shown in Figure 9. It can be seen that corrosion products are mainly composed of Al and O and the chloride is mainly present along the cracks. It can be attributed that the surface $AlCl_3$ has dissolved away during the water polishing, while some $AlCl_3$ remains inside the cracks.

3.4.3. XRD Analysis. Figure 10 shows the XRD patterns of the corrosion products on the surface of 2A12 alloy after exposure for different time. It is seen that only AlO(OH) is detected in the corrosion products during the initial three months of exposure. As the exposure test increases up to 6 months, two emerging diffraction peaks around $2\theta = 18^\circ$ and $2\theta = 20^\circ$, which are identified to be $Al(OH)_3$, are detected.

3.5. EIS Measurements. EIS is an efficient method to study the surface condition of metals and also a powerful tool for evaluating the protectiveness of the corrosion product layer formed on metals [8, 22, 26]. Figure 11 shows the time variation in EIS diagrams of the 2A12 aluminum alloy before and after exposure for 1, 6, 12, and 24 months. It is seen that all impedance spectra of the specimens consist of two capacitive loops except for that of the sample exposed for 1 month as shown in Figure 11(b). It shows that a low-frequency diffusion tail appears after immersing in the 0.1 M NaCl solution for 24 h and 48 h. This is because the surface corrosion product layer on the specimen exposed for 1 month will be destroyed after immersing in the NaCl solution for a long time. Meanwhile, the intergranular corrosion crack fronts will be activated due to the permeation of the reactant species like H_2O and O_2. Once the corrosion fronts are reactivated, there is need for abundant reactant species to support the reactions. Therefore, the diffusion tail appears because the reactant species are not sufficient to sustain the corrosion reactions under the corrosion products. For the

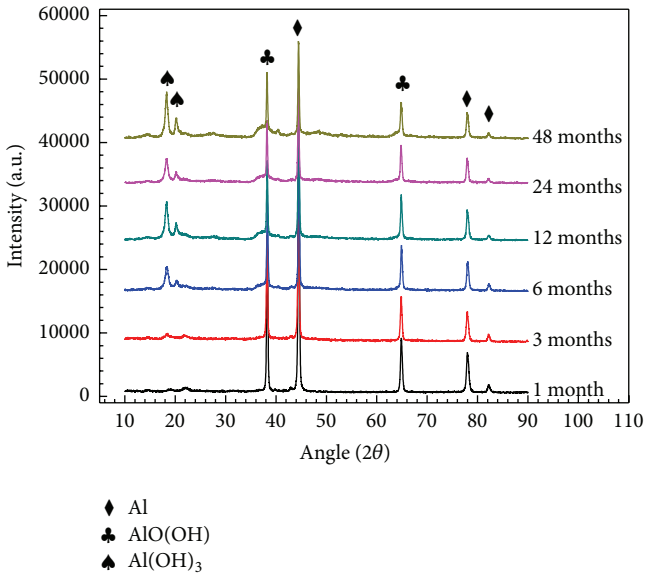

FIGURE 10: XRD patterns of the corrosion products formed on 2A12 aluminum alloy after different exposure time.

specimens exposed for 6 months or longer, the corrosion reactions under the surface layers are slow due to the thick corrosion product films. Therefore, the diffusion is not the rate controlling step and the diffusion tail does not appear.

The equivalent circuit models in Figure 12 are used to fit the EIS results in Figure 11. Among them, Model A is used to fit the spectra with two capacitive loops and Model B is used for modeling the spectra with a diffusion tail in Figure 11(b). In Model A, R_s is solution resistance; Q_f and R_f are the constant phase element of the corrosion product layer and its resistance for the corroded 2A12 and the constant phase element of the oxide film and its resistance for the freshly prepared 2A12 samples. CPE_{dl} and R_t are the double layer capacitance and the charge transfer resistance, respectively. In Model B, the redundant W is the Warburg impedance which is associated with the diffusion process through the corrosion product layer. The fitting results are also shown as solid lines in Figure 11, which match the experimental data well, indicating that the equivalent circuits in Figure 12 are suitable for fitting the EIS results.

The polarization resistance, R_p, the reciprocal of which is proportional to the corrosion rate [22], can be calculated from the two equivalent circuits as follows: $R_p = R_f + R_t$. The R_p values of 2A12 alloy before and after exposure varying with immersion time are shown in Figure 13. It is seen that the R_p values of all the corroded specimens are higher than the 2A12 substrate after immersion in the NaCl solution for only 0.5 h. This is the reason why the corrosion rate decreases in the initial exposure periods. As the immersion test extends, the R_p values of the specimen exposed for 6 months fluctuate around that of the freshly prepared sample. Meanwhile, the R_p of the samples exposed for only 1 month exhibits lower values than the specimen without exposure, while for the specimens exposed for 12 months or longer, the R_p present significantly higher values as compared with the 2A12 substrate. This may explain why the weight loss increments become ignorable in the later stage of the exposure test (Figure 4(a)).

3.6. Corrosion Morphology without Corrosion Products. The surface corrosion morphologies of 2A12 alloy after removing corrosion products are shown in Figure 14. It is observed that some pits form after exposure for 1 month (Figure 14(a)). With the increase of exposure time (Figure 14(b)), deeper and wider corrosion spots are observed and the corrosion zone almost covers the whole surface. More and more grains are corroded away, leaving a rugged surface as shown in Figure 14(c).

4. Discussion

4.1. Corrosion Kinetics of 2A12 Aluminum Alloy in Tropical Marine Atmosphere. For aluminum and aluminum alloys, a number of studies have reported the development of corrosion loss with time, both for laboratory investigation [5] and field exposure test [6, 7, 9]. Most of these studies have interpreted the data in terms of the well-known and widely applied power function [27]:

$$W = At^n, \tag{3}$$

where A and W are the corrosion losses after one and t years of exposure, respectively, and n is a constant. This equation is a simplification of the mathematical result for oxygen diffusion through increasing thickness of the corrosion films. Townsend and Zoccola [28] have proposed a method to analyze corrosion data using linear regression analysis to fit a straight line on log-log plot by taking logarithm of (3):

$$\log W = \log A + n \log t. \tag{4}$$

In this work, however, weight loss of 2A12 alloy is found to deviate from (3). This phenomenon can be easily observed in Figure 15, which reproduces the result in Figure 4(a) by plotting the weight loss against the exposure time in log-log coordinates. It is seen that the log-log plot of weight loss versus time presents two straight lines taking the 12 months of exposure as the turning point. This behavior has been reported by some researchers [29] who described this irregular corrosion behavior as in the following representative equation:

$$W = At_1^{n_1 - n_2} t^{n_2} \quad (t \geq t_1), \tag{5}$$

where t_1 is the length in months of the first period of slope n_1 and n_2 is the slope in the second period. The fitting results of the two linear segments are shown in Figure 15. It is found that the slope of the second segment (n_2) is smaller than that of the initial segment (n_1) and both of them are less than 0.5. The constant n is a significant parameter that can be considered as an indicator for the physicochemical behavior of the corrosion product layer [30]. Value of n lower than 0.5 suggests a parabolic growth of the layer by formation

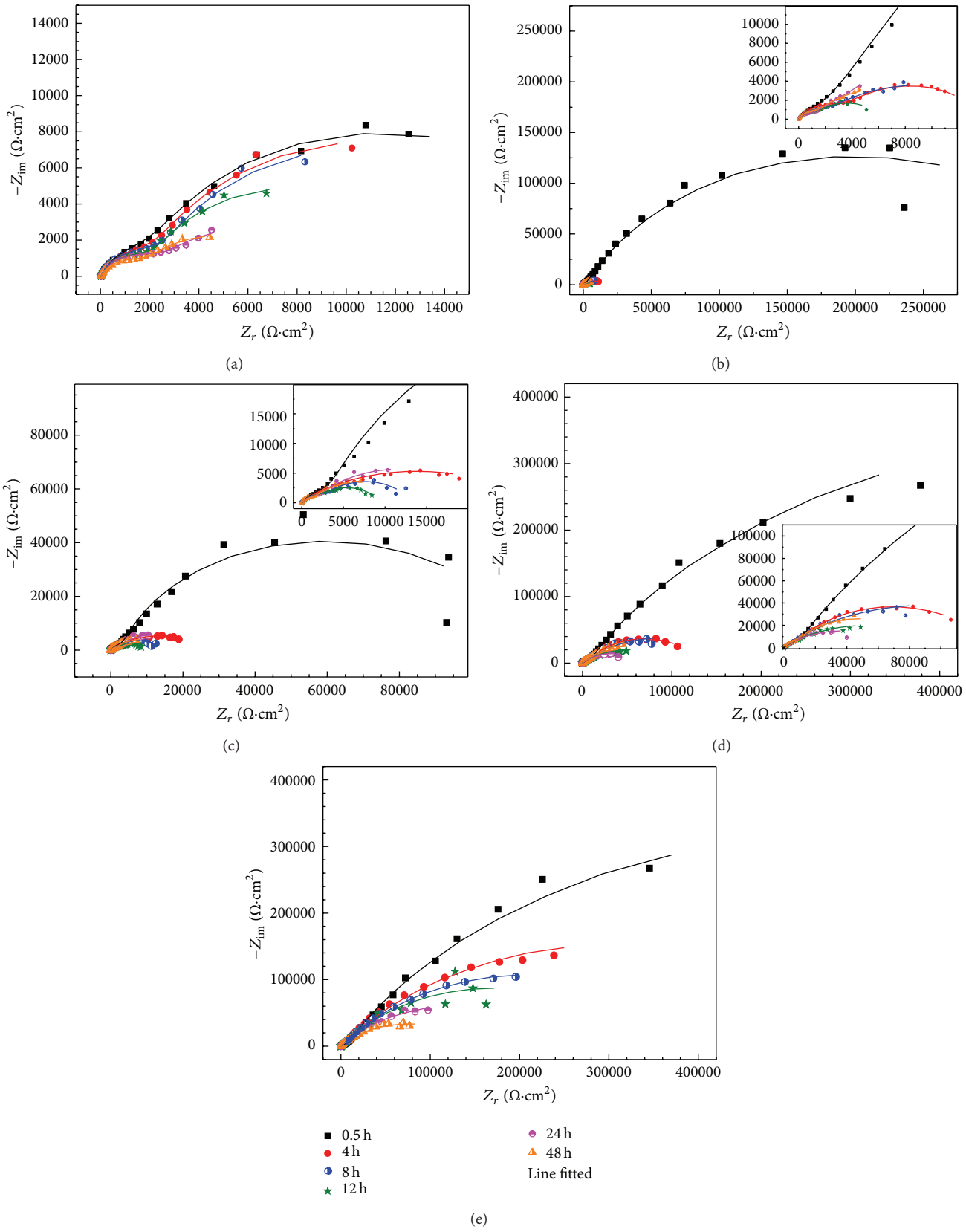

Figure 11: Nyquist diagrams for 2A12 aluminum alloy substrate (a) and specimens after exposure for 1 month (b), 6 months (c), 12 months (d), and 24 months (e) during the immersion test.

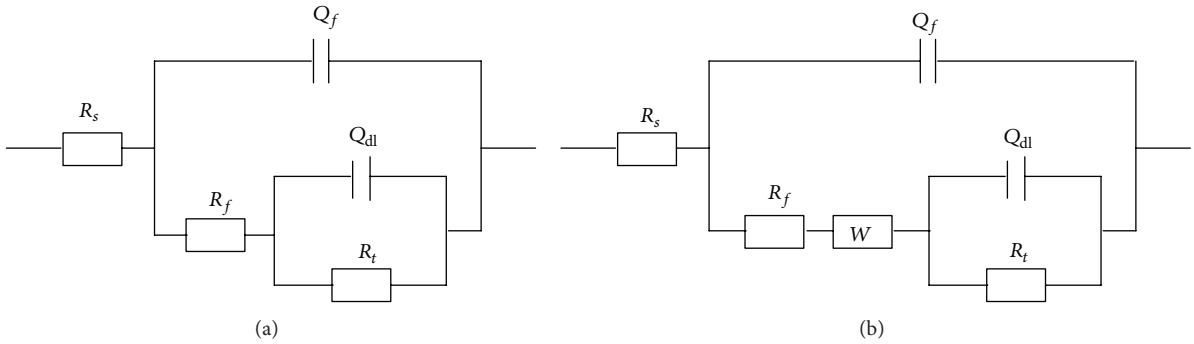

FIGURE 12: Equivalent circuits for 2A12 aluminum alloy with different exposure time in 0.1 M NaCl: (a) Model A and (b) Model B.

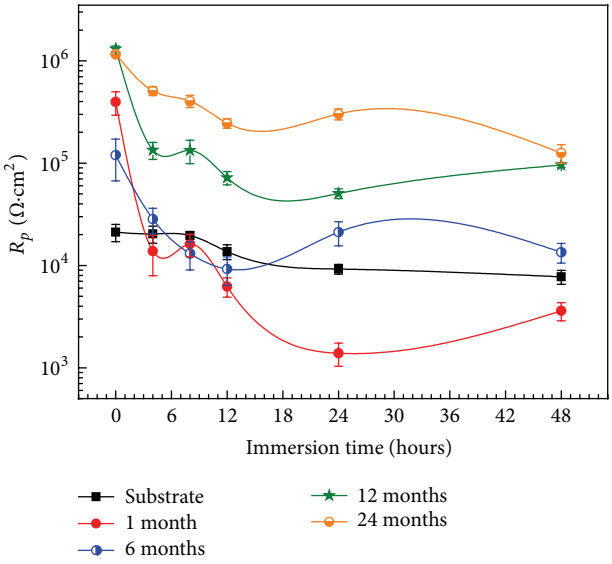

FIGURE 13: Calculated polarization resistance (R_p) of 2A12 aluminum alloy after exposure for different time.

of protective corrosion products that decrease the corrosion rate by acting as a barrier to the transportation of aggressive agents. In this work, both n_1 and n_2 are less than 0.5, which indicates that a protective corrosion product layer forms on 2A12 aluminum during the exposure test. The relatively lower value of n_2 demonstrates that corrosion products formed on 2A12 aluminum after exposure for 12 months or longer exhibit a better protectiveness, which is certified by the EIS results in the following section.

Corrosion rate of the 2A12 aluminum alloy presents a deceleration trend with some fluctuations during the exposure test. Ma et al. [29] revealed that this special behavior only occurred in marine environment because of the effect of chloride. In our previous work, the same phenomenon was also demonstrated for AZ31 magnesium in Xisha marine atmosphere [22]. It can be speculated that, in this work, the fluctuation of the corrosion rate is mainly attributed to the competition between the deterioration effect caused by chloride ions and the stabilisation process of the corrosion product layer.

4.2. Electrochemical Behavior of Corroded 2A12 Aluminum and Its Implication on the Protectiveness of Corrosion Products. EIS is an effective method to investigate the corrosion mechanism and evaluate the protectiveness of the corrosion product layer formed on metals. In our previous work [22], protectiveness of the corrosion film generated on AZ31 magnesium after atmospheric exposure was investigated by immersing the corrosion product-covered specimens in NaCl solution for different time and measuring the EIS. It illustrated that EIS data of the corroded specimens from long time immersion is more accurate than that only from immersion for a short time. In this work, the EIS measurements are also employed to characterize the protectiveness of the corrosion products based on the calculated R_f and CPE$_f$ values.

The depression of the semicircles with immersion time in Figure 8 might be caused by surface roughness and/or heterogeneities in the metal/electrolyte interface. Therefore, constant phase element (CPE) is used for more accurate analysis of impedance behavior of the electric double layer. The impedance of CPE is expressed as [8]

$$Z_{\text{CPE}} = Y_0^{-1} (j\omega)^{-n}, \tag{6}$$

where Z_{CPE} is the impedance of a CPE, Y_0 is the modulus, j is the imaginary component, ω is the angular frequency, and n is the power index number ($0 < n \leq 1$). CPE is commonly used to replace capacitance, but CPE is different from capacitance [8]. The film capacitance can be calculated from CPE parameters values (Y_0 and n) using the following expression [31]:

$$C_f = Y_0^{1/n} R_f^{(1-n)/n}, \tag{7}$$

where C_f is the film capacitance and R_f is the film resistance. The R_f, Y_0, and n values fitted from the EIS data by the equivalent circuits and the calculated C_f values are listed in Table 4.

Figure 16 shows the variation of C_f and R_f with the immersion time. The film resistance R_f represents the barrier against migration of ions in association with the corrosion reaction and is useful for estimating the protective properties of the corrosion scales [32]. A higher R_f value means higher protectiveness of the corrosion scales. So it can be speculated from Figure 13 that the corrosion scales formed on the surface

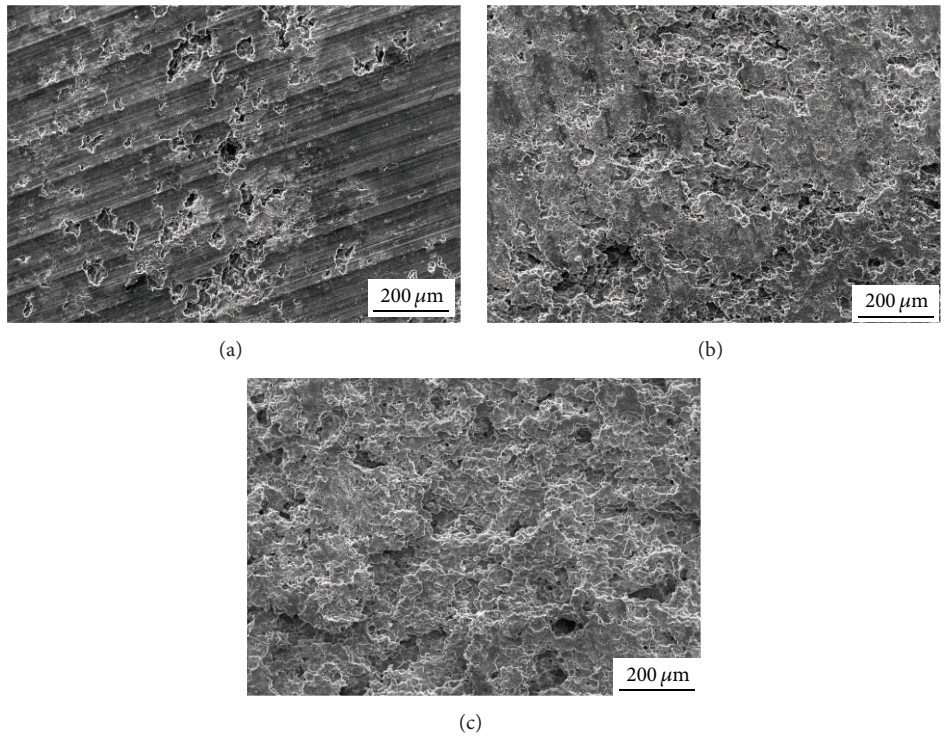

Figure 14: Corrosion morphologies of specimens without corrosion products after exposure for 1 month (a), 12 months (b), and 48 months (c).

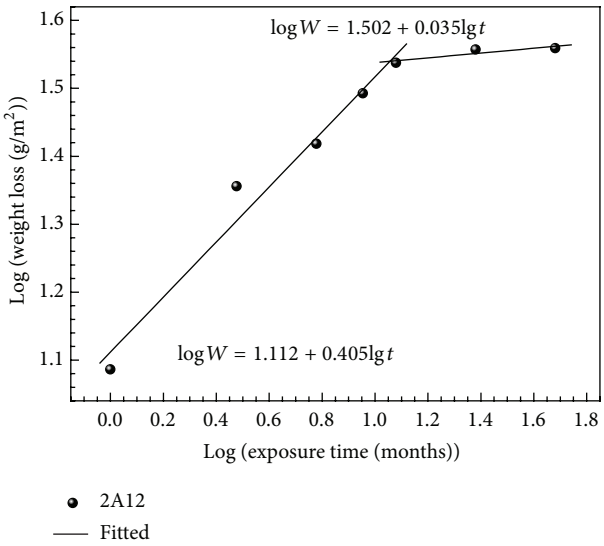

Figure 15: Bilogarithmic plots of data points from Figure 3(a) as well as the fitting lines.

of the 2A12 aluminum alloy after exposure in the tropical marine atmosphere for 12 months and 24 months have better protectiveness than the others based on the fact that they have higher R_f values. This explains why the weight loss versus exposure time plot (Figure 12) exhibits a turning point at 12 months.

The C_f value also has been used to evaluate the protective effect of the corrosion products using the parameter [8, 32]

$$C = \varepsilon\varepsilon_0 \frac{A}{d}, \tag{8}$$

where C is the capacitance, ε is the relative permittivity of the oxide, ε_0 is the vacuum permittivity, d is the thickness of the product layer, and A is the effective area which is highly dependent on the structure of the corrosion product layer. Loose and porous structure corresponds to a large A value while dense and packed structure corresponds to a small value [26]. The relative permittivity of the film, ε, is recognized as a constant because the composition change of the corrosion products can be ignored. Figure 17 compares the C_f values of the 2A12 substrate and the exposed specimens after immersion in 0.1 M NaCl solution for 0.5 h. A nonmonotonous trend of C_f value is observed, which indicates that both A and d vary during the exposure test. For the freshly prepared sample, the C_f is about one order greater in magnitude than the corrosion product covered samples, ascribed to the thin film formed during the short-term immersion. After exposure for 1 month, pitting corrosion occurs and corrosion products form on the specimen, which results in the decrease of the effective area A and the increase of the thickness d. Therefore, C_f drops sharply to a low value. With increasing of the exposure time, corrosion product layer covers the whole surface that gives rise to an increase of the effective area A. This is responsible for the large C_f of the specimen exposed for 6 months. As the exposure continues, corrosion products become denser and compact

Table 4: Values of the parameters Y_0, R_f, and n as well as the calculated C_f.

Specimens	Immersion time	Y_0 (F·cm^{-2} · s^{n-1})	n	R_f (Ω·cm^2)	C_f (F·cm^{-2})
Substrate	0.5 h	1.43×10^{-4}	0.846	4142	1.30×10^{-4}
	4 h	1.62×10^{-4}	0.853	3425	1.46×10^{-4}
	8 h	1.58×10^{-4}	0.850	3489	1.42×10^{-4}
	12 h	1.79×10^{-4}	0.880	2953	1.64×10^{-4}
	24 h	2.18×10^{-4}	0.825	2956	1.99×10^{-4}
	48 h	2.19×10^{-4}	0.827	2216	1.88×10^{-4}
1 month	0.5 h	3.1×10^{-6}	0.772	3600	8.22×10^{-7}
	4 h	2.9×10^{-5}	0.748	4248	1.43×10^{-5}
	8 h	4.76×10^{-5}	0.816	2239	2.87×10^{-5}
	12 h	1.05×10^{-4}	0.784	1486	6.29×10^{-5}
	24 h	9.76×10^{-5}	0.838	1070	6.31×10^{-5}
	48 h	1.59×10^{-4}	0.826	1867	1.23×10^{-4}
6 months	0.5 h	1.17×10^{-5}	0.689	7369	3.87×10^{-6}
	4 h	2.6×10^{-5}	0.691	3979	9.42×10^{-6}
	8 h	4.19×10^{-5}	0.717	3800	2.03×10^{-5}
	12 h	5.12×10^{-5}	0.742	3388	2.79×10^{-5}
	24 h	5.9×10^{-5}	0.796	2120	3.46×10^{-5}
	48 h	1.07×10^{-4}	0.823	1801	7.51×10^{-5}
12 months	0.5 h	6.9×10^{-6}	0.579	29280	2.15×10^{-6}
	4 h	9.6×10^{-6}	0.625	17890	3.33×10^{-6}
	8 h	1.31×10^{-5}	0.651	11240	4.68×10^{-6}
	12 h	1.33×10^{-5}	0.749	8530	6.40×10^{-6}
	24 h	1.96×10^{-5}	0.781	7677	1.15×10^{-5}
	48 h	2.05×10^{-5}	0.801	9099	1.35×10^{-5}
24 months	0.5 h	3.7×10^{-6}	0.571	13400	3.89×10^{-6}
	4 h	7.9×10^{-6}	0.606	10590	1.58×10^{-6}
	8 h	1.27×10^{-5}	0.601	44720	8.72×10^{-6}
	12 h	1.3×10^{-5}	0.626	65310	1.18×10^{-5}
	24 h	1.82×10^{-5}	0.646	25430	1.19×10^{-5}
	48 h	1.43×10^{-5}	0.704	28600	9.81×10^{-6}

accompanied with the growth of the thickness, resulting in the decrease of A and d and consequently the decrease of C_f.

As the immersion test extends, the corrosion product layer is destroyed by the aggressive chloride ions and thus the C_f value varies (Figure 16(b)). The C_f values present an increase trend with the prolonged immersion time, indicating the reduction of the layer thickness and the enlargement of the surface area. Moreover, the C_f of the specimen after 12- and 24-month exposure always keep lower values throughout the immersion test. These results once again certify the better protectiveness of the product layer generated after exposure for 12 and 24 months.

4.3. Localized Corrosion Behavior of 2A12 Aluminum Alloy in Tropical Marine Atmosphere

4.3.1. Pitting Corrosion of 2A12 Aluminum Alloy. Due to the high content of chloride ions existing in Xisha marine atmosphere, pitting of aluminum alloys is thus highly expected. When exposed to the Xisha marine atmosphere, an oxide layer composed of alumina (Al_2O_3) and boehmite (γ-AlOOH) or bayerite ($Al(OH)_3$) [6] forms on the surface of the 2A12 aluminum alloy. However, there exist many intermetallic (IM) particles, such as S-phase, θ-phase, and AlCuFeMn phase in the alloy (Figures 1 and 2). Because of the presence of the IM particles, some flaws occur in the oxide surrounding the IM particles which are preferentially attacked by chloride ions and leading to the initiation of pitting corrosion. The galvanic coupling effect between the IM particles and the surrounding matrix promotes the growth of the pits.

4.3.2. Intergranular Corrosion of 2A12 Aluminum Alloy. IGC (intergranular corrosion) is detected on the 2A12 aluminum alloy during exposure in Xisha atmosphere. It is recognized that IGC is caused by the formation of a microgalvanic cell between the grain matrix and the grain boundary region, which includes the grain boundary precipitates and the precipitate-free zone. In this work, no obvious PFZ is detected in 2A12 aluminum alloy by TEM. Therefore, the grain boundary precipitates shown in Figure 2 are mainly responsible for the IGC propagation. According to Buchheit

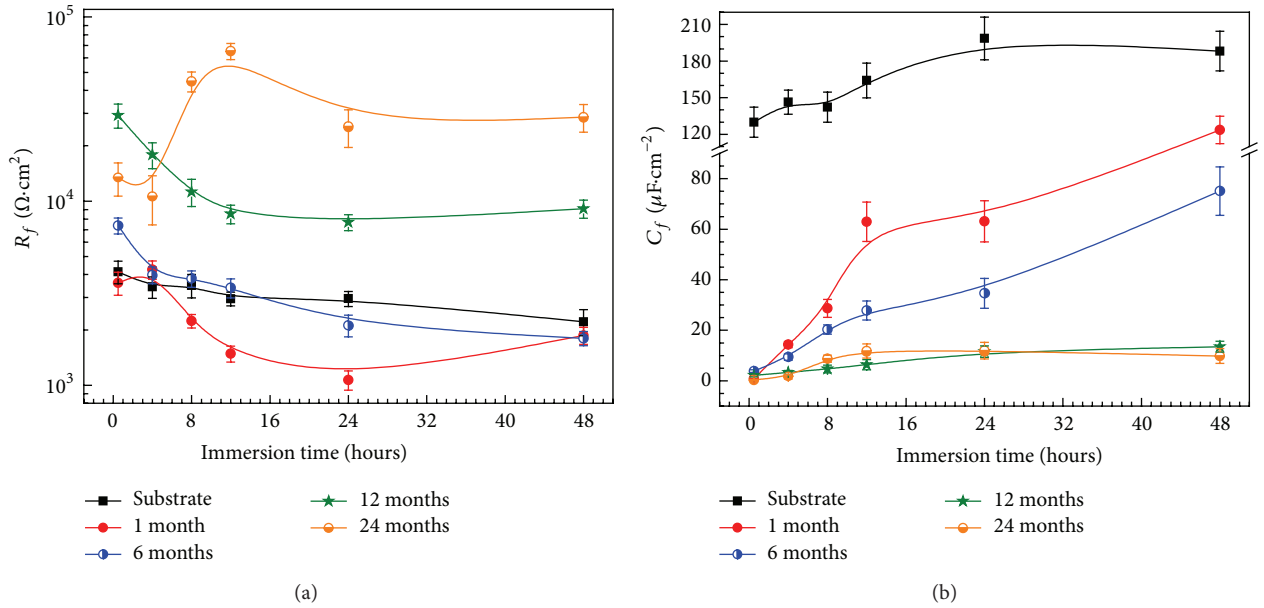

FIGURE 16: Fitting results of film resistance R_f (a) and the calculated capacity C_f (b) of the corrosion product layer during immersion test.

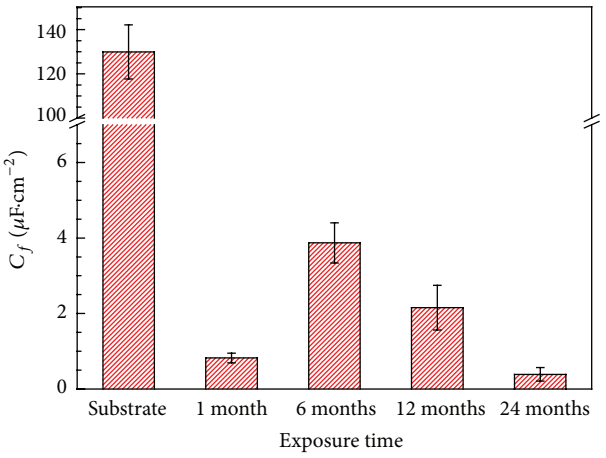

FIGURE 17: The calculated capacity C_f of the corrosion products after immersion in 0.1 M NaCl for 0.5 h.

[33, 34] and other researchers [35, 36], the *S*-phase particles (Al_2CuMg) are anodic with respect to the adjacent grains and can be expected to undergo preferential dissolution, leading to acidification of the anolyte solution through hydrolysis of aluminum ions in the intergranular crevice and also to copper enrichment on the surface of the grain crevice behind the active anodic head at the point of attack. In comparison, the *T*-phase particles ($Al_{20}Cu_2Mn_3$) are also anodic with respect to the matrix [36] and might preferentially dissolve. Due to the dissolution of the grain boundary precipitates, an anodic path along the grain boundaries forms, resulting in the propagation of IGC. Besides, IGC is thought to have a more detrimental effect on fatigue life than pits as it can act as a more severe stress raiser [37]. Therefore, the mechanical properties reduce heavily as shown in Figure 5.

5. Conclusion

Corrosion behavior of 2A12 aluminum alloy in a tropical marine atmosphere was investigated in this work. The main conclusions were made as follows:

(1) The weight loss of 2A12 aluminum alloy exposed to the tropical marine environment deviates from the well-known bilogarithmic equation $W = At^n$.

(2) The weight loss versus exposure time plot presents two segments, taking the 12 months as turning point. The slope of the second segment is significantly lower than that of the first segment, which is attributed to the good protectiveness of the corrosion product layer.

(3) Mechanical properties of the 2A12 alloy decrease heavily as the exposure time extends.

(4) The protectiveness of corrosion products formed on 2A12 aluminum after atmospheric exposure varies with the exposure time. Corrosion products formed after exposing for 12 and 24 months present better barrier effect against further attacks.

(5) Pitting corrosion and intergranular corrosion occur on 2A12 aluminum alloy in this tropical marine atmosphere, resulting in the deterioration of the mechanical properties during the exposure.

Conflict of Interests

The authors declare that there is no conflict of interests regarding the publication of this paper.

Acknowledgments

The authors wish to acknowledgement the financial support of the National Basic Research Program of China (973 Program Project no. 2014CB643300) and the National Science and Technology Basic Project of the Ministry of Science and Technology of China (no. 2012FY113000).

References

[1] A. Heinz, A. Haszler, C. Keidel, S. Moldenhauer, R. Benedictus, and W. S. Miller, "Recent development in aluminium alloys for aerospace applications," *Materials Science and Engineering A*, vol. 280, no. 1, pp. 102–107, 2000.

[2] T. Dursun and C. Soutis, "Recent developments in advanced aircraft aluminium alloys," *Materials and Design*, vol. 56, pp. 862–871, 2014.

[3] T. E. Graedel, "Corrosion mechanisms for aluminum exposed to the atmosphere," *Journal of the Electrochemical Society*, vol. 136, no. 4, pp. 204C–212C, 1989.

[4] S. Sun, Q. Zheng, D. Li, S. Hu, and J. Wen, "Exfoliation corrosion of extruded 2024-T4 in the coastal environments in China," *Corrosion Science*, vol. 53, no. 8, pp. 2527–2538, 2011.

[5] D. B. Blücher, R. Lindström, J.-E. Svensson, and L.-G. Johansson, "The effect of CO_2 on the NaCl-induced atmospheric corrosion of aluminum," *Journal of the Electrochemical Society*, vol. 148, no. 4, pp. B127–B131, 2001.

[6] D. de la Fuente, E. Otero-Huerta, and M. Morcillo, "Studies of long-term weathering of aluminium in the atmosphere," *Corrosion Science*, vol. 49, no. 7, pp. 3134–3148, 2007.

[7] B. B. Wang, Z. Y. Wang, W. Han, and W. Ke, "Atmospheric corrosion of aluminium alloy 2024-T3 exposed to salt lake environment in Western China," *Corrosion Science*, vol. 59, pp. 63–70, 2012.

[8] Y. Liu, Z. Wang, and W. Ke, "Study on influence of native oxide and corrosion products on atmospheric corrosion of pure Al," *Corrosion Science*, vol. 80, pp. 169–176, 2014.

[9] S. Sun, Q. Zheng, D. Li, and J. Wen, "Long-term atmospheric corrosion behaviour of aluminium alloys 2024 and 7075 in urban, coastal and industrial environments," *Corrosion Science*, vol. 51, no. 4, pp. 719–727, 2009.

[10] Z. Szklarska-Smialowska, "Pitting corrosion of aluminum," *Corrosion Science*, vol. 41, no. 9, pp. 1743–1767, 1999.

[11] J. R. Vilche, F. E. Varela, G. Acuña et al., "A survey of Argentinean atmospheric corrosion: I—aluminium and zinc samples," *Corrosion Science*, vol. 37, no. 6, pp. 941–961, 1995.

[12] G. S. Chen, M. Gao, and R. P. Wei, "Microconstituent-induced pitting corrosion in aluminum alloy 2024-T3," *Corrosion*, vol. 52, no. 1, pp. 8–15, 1996.

[13] S. C. Wang and M. J. Starink, "Two types of S phase precipitates in Al–Cu–Mg alloys," *Acta Materialia*, vol. 55, no. 3, pp. 933–941, 2007.

[14] Z. Q. Feng, Y. Q. Yang, B. Huang, M. H. Li, Y. X. Chen, and J. G. Ru, "Crystal substructures of the rotation-twinned T ($Al_{20}Cu_2Mn_3$) phase in 2024 aluminum alloy," *Journal of Alloys and Compounds*, vol. 583, pp. 445–451, 2014.

[15] R. Buchheit, R. Grant, P. Hlava, B. McKenzie, and G. Zender, "Local dissolution phenomena associated with S Phase (Al_2CuMg) particles in aluminum alloy 2024–T3," *Journal of The Electrochemical Society*, vol. 144, pp. 2621–2628, 1997.

[16] Z. Y. Cui, X. G. Li, K. Xiao, C. F. Dong, Z. Y. Liu, and L. W. Wang, "Corrosion behavior of field-exposed zinc in a tropical marine atmosphere," *Corrosion*, vol. 70, no. 7, pp. 731–748, 2014.

[17] E. Schindelholz, R. G. Kelly, I. S. Cole, W. D. Ganther, and T. H. Muster, "Comparability and accuracy of time of wetness sensing methods relevant for atmospheric corrosion," *Corrosion Science*, vol. 67, pp. 233–241, 2013.

[18] I. S. Cole, W. D. Ganther, J. D. Sinclair, D. Lau, and D. A. Paterson, "A study of the wetting of metal surfaces in order to understand the processes controlling atmospheric corrosion," *Journal of the Electrochemical Society*, vol. 151, no. 12, pp. B627–B635, 2004.

[19] I. S. Cole and W. D. Ganther, "Experimental determination of duration of wetness on metal surfaces," *Corrosion Engineering Science and Technology*, vol. 43, no. 2, pp. 156–162, 2008.

[20] ISO 9223, "Corrosion of metals and alloys—classification of corrosivity of atmospheres," 1992.

[21] ISO 9225, Corrosion of metals and alloys—corrosivity of atmospheres—measurement of pollution, 1992.

[22] Z. Y. Cui, X. G. Li, K. Xiao, and C. F. Dong, "Atmospheric corrosion of field-exposed AZ31 magnesium in a tropical marine environment," *Corrosion Science*, vol. 76, pp. 243–256, 2013.

[23] Z. Dan, I. Muto, and N. Hara, "Effects of environmental factors on atmospheric corrosion of aluminium and its alloys under constant dew point conditions," *Corrosion Science*, vol. 57, pp. 22–29, 2012.

[24] N. D. Alexopoulos and P. Papanikos, "Experimental and theoretical studies of corrosion-induced mechanical properties degradation of aircraft 2024 aluminum alloy," *Materials Science and Engineering A*, vol. 498, no. 1-2, pp. 248–257, 2008.

[25] N. D. Alexopoulos, "On the corrosion-induced mechanical degradation for different artificial aging conditions of 2024 aluminum alloy," *Materials Science and Engineering A*, vol. 520, no. 1-2, pp. 40–48, 2009.

[26] J. Wang, Z. Y. Wang, and W. Ke, "A study of the evolution of rust on weathering steel submitted to the Qinghai salt lake atmospheric corrosion," *Materials Chemistry and Physics*, vol. 139, no. 1, pp. 225–232, 2013.

[27] M. Benarie and F. L. Lipfert, "A general corrosion function in terms of atmospheric pollutant concentrations and rain pH," *Atmospheric Environment*, vol. 20, no. 10, pp. 1947–1958, 1986.

[28] H. E. Townsend and J. C. Zoccola, "Eight-year atmospheric corrosion performance of weathering steel in industrial, rural and marine environments," in *Atmospheric Corrosion*, ASTM STP 767, p. 45, ASTM, Philadelphia, Pa, USA, 1982.

[29] Y. Ma, Y. Li, and F. Wang, "Corrosion of low carbon steel in atmospheric environments of different chloride content," *Corrosion Science*, vol. 51, no. 5, pp. 997–1006, 2009.

[30] D. de la Fuente, I. Díaz, J. Simancas, B. Chico, and M. Morcillo, "Long-term atmospheric corrosion of mild steel," *Corrosion Science*, vol. 53, no. 2, pp. 604–617, 2011.

[31] B. Hirschorn, M. E. Orazem, B. Tribollet, V. Vivier, I. Frateur, and M. Musiani, "Determination of effective capacitance and film thickness from constant-phase-element parameters," *Electrochimica Acta*, vol. 55, no. 21, pp. 6218–6227, 2010.

[32] Y. Ma, Y. Li, and F. Wang, "The effect of β-FeOOH on the corrosion behavior of low carbon steel exposed in tropic marine environment," *Materials Chemistry and Physics*, vol. 112, no. 3, pp. 844–852, 2008.

[33] R. G. Buchheit, "A compilation of corrosion potentials reported for intermetallic phases in aluminum alloys," *Journal of the Electrochemical Society*, vol. 142, no. 11, pp. 3994–3996, 1995.

[34] R. G. Buchheit, L. P. Montes, M. A. Martinez, J. Michael, and P. F. Hlava, "The electrochemical characteristics of bulk–synthesized Al_2CuMg," *Journal of the Electrochemical Society*, vol. 146, no. 12, pp. 4424–4428, 1999.

[35] C. Blanc, A. Freulon, M.-C. Lafont, Y. Kihn, and G. Mankowski, "Modelling the corrosion behaviour of Al_2CuMg coarse particles in copper-rich aluminium alloys," *Corrosion Science*, vol. 48, no. 11, pp. 3838–3851, 2006.

[36] S. M. Skolianos, T. Z. Kattamis, and O. F. Devereux, "Microstructure and corrosion behavior of as-cast and heat-treated Al-4.5 Wt pct Cu-2.0 wt pct Mn alloys," *Metallurgical Transactions A*, vol. 20, no. 11, pp. 2499–2516, 1989.

[37] J. R. Davis, *Corrosion of Aluminum and Aluminum Alloys*, ASM International, 1999.